

# NUMERICAL STUDY ON HEAT TRANSFER CHARACTERISTICS OF NANOFUID BASED NATURAL CIRCULATION LOOP

**RAMESH BABU BEJJAM, KIRAN KUMAR K\***

Department of Mechanical Engineering, National Institute of Technology Warangal, Telangana, India

Corresponding author: kkirankumar2000@gmail.com

*In this paper the steady-state analysis has been carried out on single phase natural circulation loop with water and water based  $Al_2O_3$  ( $Al_2O_3$ /water) nanofluid at 1%, 3%, 5% and 6% particle volume concentrations. For this study, a three-dimensional geometry of natural circulation loop is developed and simulated by using the software, ANSYS (FLUENT) 14.5. Based on the Stokes number, mixture model is adopted to simulate the nanofluid based natural circulation loop. For the simulations, the imposed thermal boundary conditions are: constant heat input over the range of 200-1000W with step size of 200W at the heat source and isothermal wall temperature of 293K at the heat sink. Adiabatic boundary condition is imposed to the riser and downcomer. The heat transfer characteristics and fluid flow behaviour of the loop fluid in natural circulation loop for different heat inputs and particle concentrations are presented. The result shows that the mass flow rate of loop fluid in natural circulation loop is enhanced by 26% and effectiveness of the natural circulation loop is improved by 15% with  $Al_2O_3$ /water nanofluid when compared with water. All the simulation results are validated with the open literature in terms of Reynolds number and modified Grashof number. These comparisons confidently say that the present 3-D numerical model could be useful to estimate the performance of natural circulation loop.*

*Key words: Heat transfer, Natural circulation, Nanofluid, Computational fluid dynamics, Mixture model*

## 1. Introduction

Natural circulation loop (NCL) is a passive heat transfer arrangement to transfer heat from a source to a sink without any mechanical aid. Therefore, it offers some unique and distinctive applications such as solar water heaters, geothermal heat extraction systems, new generation nuclear reactors, electronic cooling systems and refrigeration systems etc. By imposing the temperature gradient between source and sink, the density ( $\rho$ ) difference is developed in the loop fluid which causes the fluid to circulate in the NCL. The absence of mechanical elements gives advantages such as high reliability, safety and low maintenance cost to NCL over forced circulation loop.

It is clear from the literature that most of the numerical studies and experimental investigations are carried out on symmetrically heated and cooled loops. Zvirin [1] studied the suitability of the NCLs in various heat extraction systems and new correlations are developed for the temperature rise at the source or temperature drop at the sink and steady state mass flow rate. Vijayan et al. [2] studied the effects of heat source and heat sink orientations on the stability of the rectangular NCL. They concluded that more stability is observed with vertical configuration of the heat source

and the heat sink. Experimental investigations on the stability characteristics of the NCLs at various loop pipe internal diameters have done by Vijayan et al. [3]. Basu et al. [4] have been proposed an analytical solution for four different loop configurations under steady-state with identical boundary and operating conditions, they concluded that the rectangular NCL model has a stable flow. In the extended work [5], they numerically analyzed the impact of geometrical parameters on the stability of NCL under steady state condition and it is concluded that stabilities can be suppressed by increasing the loop height because of more buoyancy effect. They also found that NCL with a smaller pipe diameter have more stability due to enhancement in friction. The NCL with wider loop and a longer heat source section have more stability. Kiran Kumar et al. [6] numerically evaluated the 1-D rectangular NCL under steady state for low temperature applications with hot and cold heat exchangers at the source and the sink respectively, and they developed new relation for suitability of various fluids in NCL in terms of pipe diameters and temperature rise/drop. Yadav et al. [7] numerically analyzed the performance of NCL under steady state condition with water and CO<sub>2</sub> as loop fluids. Their investigation reveals that, at pseudo-critical region the NCL with CO<sub>2</sub> exhibits seven times higher heat transfer rate than water at atmospheric condition. They also proposed new correlations for CO<sub>2</sub> based NCL. Recently, Jayaraj et al. [8] reported studies on the steady state and transient characteristics of the rectangular NCL with water. In their study, simulations are carried out on a 3-D NCL model using CFD. They described the stability behaviour of the loop fluid in NCL with different heat source and heat sink orientations.

In the NCL, thermo-physical properties of the loop fluid plays a key role on its performance. Advancements in the nanotechnology opens a gateway to new generation fluids for heat transfer applications. By suspending the nanoparticles in the working fluid at low concentrations significantly alters the thermal conductivity and consequent heat transfer properties. In the past several years, nanofluids are widespread for various industrial and commercial applications such as refrigerators, electronics cooling, solar collectors, different heat exchangers, and nuclear reactor cooling. Nayak et al. [9] experimentally investigated the flow behaviour in NCL with Al<sub>2</sub>O<sub>3</sub>/water nanofluid. They reported that flow rates are improved and flow instabilities can be suppressed with nanofluid. Recently Doganay et al. [10] experimentally examined the performance of nanofluid based natural circulation mini loop. They found that system is thermally stable at all inclination angles and at all particle volume concentrations. Effectiveness of the NCL is enhanced proportionally with particle concentration and inclination angle.

3-D modelled geometry is essential to estimate the system performance by considering some critical parameters such as influence of local buoyancy, bends in geometry and axial conductions. Though few studies based on the 3-D CFD model are available in the literature, they have certain limitations due to the assumptions made during analysis. The present study aims to numerically investigate the influence of heat transfer and rheological characteristics of water based Al<sub>2</sub>O<sub>3</sub> (Al<sub>2</sub>O<sub>3</sub>/water) nanofluid on the performance of rectangular NCL by using mixture model. For this study, 3-D modelling and simulations are carried out with Ansys-14.5 CFD package.

## **2. Numerical methodology**

The schematic diagram of rectangular NCL with riser, downcomer, source and sink is shown in fig. 1. The loop fluid is heated at the source with constant heat flux condition and cooled at the sink by isothermal wall temperature condition. A buoyancy effect created by the temperature gradients

causes to circulate the fluid in the loop. The geometrical parameters and material specifications are given in tab. 1. The following assumptions are made to while formulating the model in Ansys-Fluent 14.5. The loop is operated in steady state mode, no slip boundary condition is applied near the walls, riser and down comer sections are fully adiabatic, the nanofluid is incompressible, the nanoparticles have uniform size and shape.

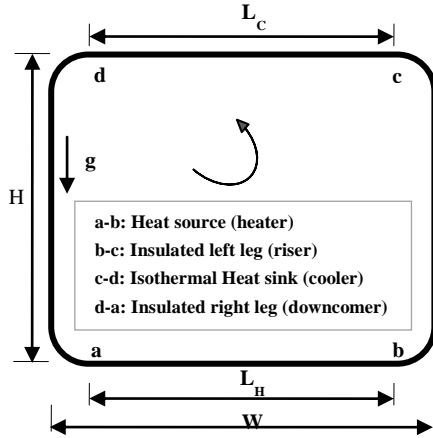


**Figure 1. Schematic diagram of the geometrical NCL model**

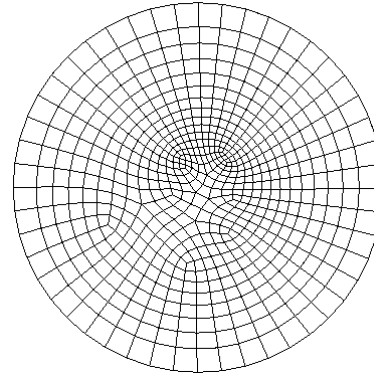


**Figure 2. Meshing of a cross section of the loop fluid**

**Table 1. Geometric specifications of the model**

Parameter	Value (unit)
Diameter of the loop	0.015 (m)
Loop pipe wall thickness	0.0016 (m)
Total length of the loop ( $L_t$ )	5.44 (m)
Length of the heat source ( $L_H$ )	1.4 (m)
Length of the heat sink ( $L_C$ )	1.4 (m)
Loop height (H)	1.26 (m)
Width of the loop (W)	1.46 (m)
Loop wall material	copper

### 2.1 Governing equations

The conservation equations of mixture model are solved using the commercial software, ANSYS (FLUENT) 14.5. The continuity, momentum and energy equations of mixture model are as follows:

Continuity equation:  $\nabla \cdot (\rho_m \vec{V}_m) = 0$  (1)

where,  $\rho_m$  and  $\vec{V}_m$  are  $\rho_m = \phi_p \rho_p + \phi_w \rho_w$  (2)

$$\vec{V}_m = \frac{\phi_p \rho_p \vec{V}_p + \phi_w \rho_w \vec{V}_w}{\rho_m} \quad (3)$$

Momentum equation:

$$\nabla \cdot (\rho_m \vec{V}_m \vec{V}_m) = -\nabla p + \nabla \cdot [\mu_m (\nabla \vec{V}_m + \nabla \vec{V}_m^T)] + (\rho_m \vec{g}) + \vec{F} + \nabla \cdot (\phi_w \rho_w \vec{V}_{dr,w} \vec{V}_{dr,w} + \phi_p \rho_p \vec{V}_{dr,p} \vec{V}_{dr,p}) \quad (4)$$

where,  $\mu_m$ ,  $\vec{V}_{dr,w}$  and  $\vec{V}_{dr,p}$  are expressed as  $\mu_m = \sum_{k=1}^n \phi_k \mu_k$  (5)

$$\vec{V}_{dr,w} = \vec{V}_w - \vec{V}_m \quad (6)$$

$$\vec{V}_{dr,p} = \vec{V}_p - \vec{V}_m \quad (7)$$

$$\text{Energy equation: } \nabla \cdot \left( \left( \phi_w \vec{V}_w (\rho_w h_w + p) \right) + \left( \phi_p \vec{V}_p (\rho_p h_p + p) \right) \right) = \nabla \cdot (K_{\text{eff}} \nabla T) \quad (8)$$

$$\text{where, } k_{\text{eff}} \text{ is expressed as } K_{\text{eff}} = \phi_p (K_p + K_t) + \phi_w (K_w + K_t) \quad (9)$$

$$C_{p,m} = \phi_p C_{p,p} + \phi_w \rho C_{p,w} \quad (10)$$

In the present study, the RNG  $k - \varepsilon$  turbulence model is considered if the flow is in the turbulent flow regime. The energy dissipation rate ' $\varepsilon$ ' and the turbulent kinetic energy ' $k$ ' are obtained by solving the following transport equations.

$$\text{Turbulent kinetic energy: } \frac{\partial}{\partial x_i} (\rho k u_i) - \frac{\partial}{\partial x_j} \left( \alpha_k \mu_{\text{eff}} \frac{\partial k}{\partial x_j} \right) = G_k + G_b - \rho \varepsilon \quad (11)$$

Turbulent energy dissipation rate:

$$\frac{\partial}{\partial x_i} (\rho \varepsilon u_i) - \frac{\partial}{\partial x_j} \left( \alpha_\varepsilon \mu_{\text{eff}} \frac{\partial \varepsilon}{\partial x_j} \right) = \left( C_{1\varepsilon} \frac{\varepsilon}{k} (G_k + C_{3\varepsilon} G_b) \right) - \left( \rho \left( C_{2\varepsilon} + \frac{C_\mu \eta^5 (1 - \eta/\eta_0)}{1 + 0.012 \eta^5} \right) \frac{\varepsilon^2}{k} \right) \quad (12)$$

where values of the model constants  $C_{1\varepsilon}$ ,  $C_{2\varepsilon}$ ,  $C_\mu$ ,  $\alpha_\varepsilon$ ,  $\alpha_k$  are 1.42, 1.68, 0.09, 1.0, 1.3 respectively and  $\eta = Sk/\varepsilon$ ,  $\eta_0 = 4.38$ .

$$\text{The Stokes number can be estimated by } St = \frac{\tau_p}{t_s} \quad (13)$$

$$\text{where, the particle response time } (\tau_p) \text{ is expressed as } \tau_p = \frac{\rho_p d_p^2}{18 \mu_w} \quad (14)$$

$$\text{and the system response time } (t_s) \text{ is obtained by } t_s = \frac{L_s}{V_s} \quad (15)$$

The modified Grashof number ( $Gr_m$ ) and Reynolds number (Re) are obtained by,

$$Gr_m = \frac{g \beta d^3 \rho^2 Q H}{A_{cs} \mu^3 C_p} \quad (16)$$

$$Re = \frac{4 \dot{m}}{\pi d \mu} \quad (17)$$

At the considered cross section, the steady state mass flow rate ( $\dot{m}$ ) and local bulk temperature of the loop fluid ( $T$ ) can be estimated by:

$$\dot{m} = \int_0^A \rho V dA \quad (18)$$

$$T = \frac{\int_0^A C_p T \rho V dA}{\int_0^A C_p \rho V dA} \quad (19)$$

Also, the friction factor ( $f$ ) is expressed as:

$$f = \frac{\pi^2 \rho \Delta p d^5}{8 \dot{m}^2 x} \quad (20)$$

Where, ' $\Delta p$ ' is the total pressure drop in the pipe at length ' $x$ '.

## 2.2 Boundary conditions

For the simulations, the imposed thermal boundary conditions are, constant heat input over the range of 200-1000W with step size of 200W is applied at heat source, isothermal wall temperature of 293K is considered at the heat sink. Riser and downcomer are considered as insulated.

## 2.3 Solution technique

Stokes number is a non-dimensional number to characterise the behaviour of particle suspended in a fluid flow. Stokes number (St) is helpful in choosing an appropriate model among

volume of fluid (VOF), mixture and eulerian models approach to simulate nanofluid flows. If  $St > 1$ , the eulerian model is most suitable and if  $St \ll 1$  or  $St \approx 1$ , any of the model can be used [11]. If stokes number is much less than 1, then the flow is viscous dominating flow. If the particle response time is much higher, then the particles will flow through the fluid without much deflection. The particle motion and fluid motions are tightly coupled and closely stream lined. But the mixture model is computationally inexpensive and widely used to simulate nanofluid flows. In the present study the  $St$  is estimated using eq. (13) and its value around  $12 \times 10^{-4}$  and hence mixture model is employed to simulate nanofluid based NCL. Rashid et al. [12] made a comparison between these models and reported that two phase models are more viable. In particular, mixture model gave close approximation with the experimental results.

A 3-D geometric model of the NCL is developed in ANSYS-14.5 geometric module and simulates with water and  $Al_2O_3$ /water nanofluid. The entire simulations are carried out at steady state condition. The implicit coupled condition is imposed. The governing equations are discretized by the finite volume method. Semi implicit method for pressure linked equations (SIMPLE) algorithm is used to couple the pressure and velocity. The moment and energy equations are iterated by using the second order upwind scheme. The turbulence effect is induced to the loop fluid if the flow is in turbulent regime by applying RNG  $k-\epsilon$  model [13] and the standard wall function condition. The turbulence kinetic energy and turbulence dissipation rates are iterated by second-order upwind scheme. The pressure term in the moment equation is solved by pressure staggering option (PRESTO) scheme. To neglect the influence of boundary layer at pipe walls, no-slip boundary condition is applied. Axial conduction along the pipe wall and viscous dissipation rate of the loop fluid are incorporated. The continuity, moment equations are converged by reaching the velocity and pressure residuals to  $10^{-3}$  and the energy equation is converged when its residual reaches to  $10^{-6}$ .

### 3. Properties of water and $Al_2O_3$ nanoparticle

Thermo-physical properties of water and  $Al_2O_3$  nanoparticle are listed in tab. 2.

**Table 2. Thermo-physical properties of water and  $Al_2O_3$  nanoparticle at 298 K**

Property (unit)	Water (from NIST)	$Al_2O_3$ nanoparticle
Density ( $kg/m^3$ )	997.05	3900
Specific heat (J/kg K)	4181.3	785.21
Thermal conductivity (W/m K)	0.60652	37.17539
Viscosity (N-s/m <sup>2</sup> )	0.00089002	---

**Table 3. Mesh result details**

Number of elements	Number of nodes	$\Delta T_{\text{heat source}}$	m (kg/s)
782784	918684	11.319	0.008799
150920	133280	11.30	0.008779
72350	65304	11.199	0.008668
48000	48960	11.101	0.008535
27250	39240	10.983	0.008412

### 4. Mesh sensitivity analysis

The meshing of the loop fluid at a cross section of the heat source is shown in fig. 2. Stern et al. [14] proposed a method for mesh verification. As on refining the element size, number of elements in the mesh are increased. This element size takes part of vital role on the simulation results. Therefore, in order to test the mesh sensitivity, five different element sizes are considered and the results are analyzed. For the mesh sensitivity test, the simulations are carried out with water at 600W

of heat input. Fig. 3 shows the influence of a number of elements on two independent variables such as steady state mass flow rate and temperature difference of the loop fluid across the heat source. The effect of a number of elements on the temperature gradient and mass flow rate is presented in tab. 3. By increasing the number of elements from 150920 to 782784, the temperature gradient across the heat source is reformed by 0.16% and the mass flow rate is refined by 0.13% only. Therefore, the mesh with 150920 number of elements is considered for the simulations in order to save the computational time and utilization of the resources.

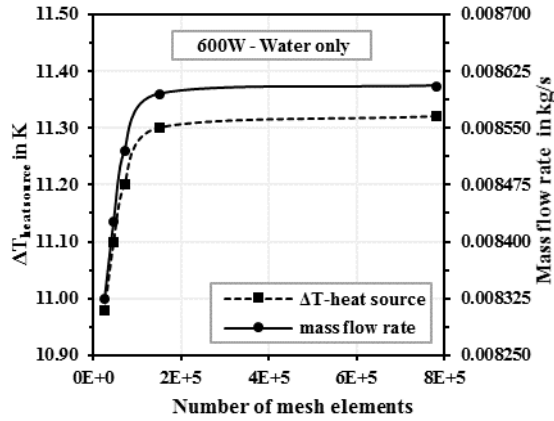


Figure 3. Mesh sensitivity analysis

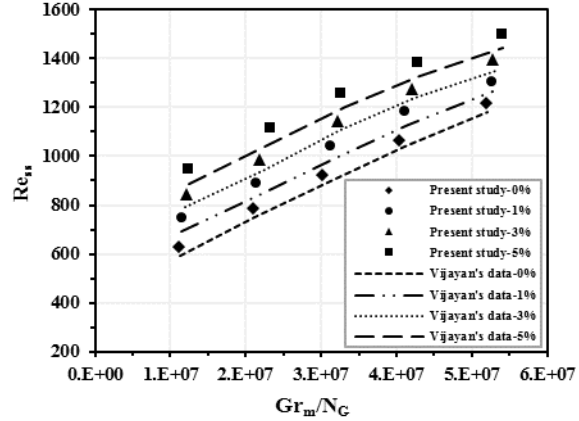


Figure 4. Validation of CFD results with Vijayan's data [15]

## 5. Results and discussion

In the present study, the simulations are carried out for various heat inputs (200-1000W) at the heat source and constant wall temperature of 293K at the heat sink. The NCL is operated with  $Al_2O_3$ /water nanofluid as loop fluid at different particle volume concentrations of 1%, 3%, 5% and 6%, and the performance is compared with water as loop fluid.

### 5.1 Validation

To validate the 3-D NCL model, the simulations are carried out at steady state condition and the results are compared with the analytical results calculated from Vijayan's correlation (eq. 21) for laminar flow [15]. However, it is to be noted that Vijayans correlation is given for single phase fluids. Hence for the comparison all thermophysical properties are calculated based on the homogeneous mixture model at bulk mean temperature. Fig. 4 illustrates that, the simulation results are well matched with analytical results over a range of Reynolds number for both water and nanofluid at different concentrations. The maximum difference between the simulation and analytical results is less than 5% for water and 10% for  $Al_2O_3$ /water nanofluid. Therefore, further analysis is carried out with the developed model. For fully laminar flow the steady state Reynolds number can be estimated using eq. (21).

$$Re_{ss} = 0.1768 \left[ \frac{Gr_m}{N_C} \right]^{0.5} \quad (21)$$

### 5.2 Temperature contours for water and $Al_2O_3$ /water nanofluid at 600W of heat input and 3% concentration

Figs. 5(i) and 5(ii) show the temperature contours for water and  $Al_2O_3$ /water nanofluid at the center of heat source, riser, heat sink, and down comer respectively. Due to the buoyancy effect relatively more temperature is observed at the top portion of the pipe in horizontal sections such as heat source and sink. In case of riser and downcomer, more uniform temperature profiles are observed throughout the cross section by considering adiabatic wall condition. High temperatures are observed in case of  $Al_2O_3$ /water nanofluid.

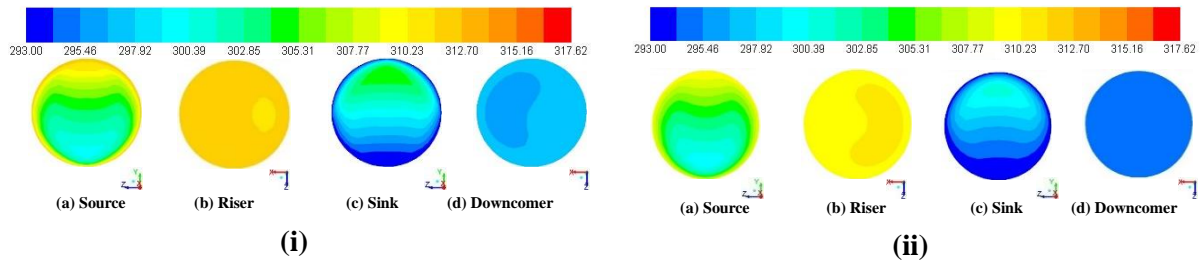


**Figure 5. Temperature contours at 600W (i) for water (ii)  $Al_2O_3$ /water nanofluid ( $\phi = 3\%$ )**

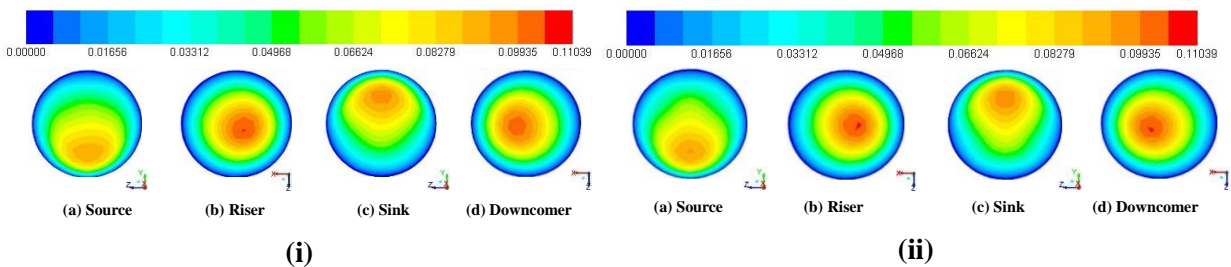


**Figure 6. Velocity contours at 600W (i) for water (ii)  $Al_2O_3$ /water nanofluid ( $\phi = 3\%$ )**

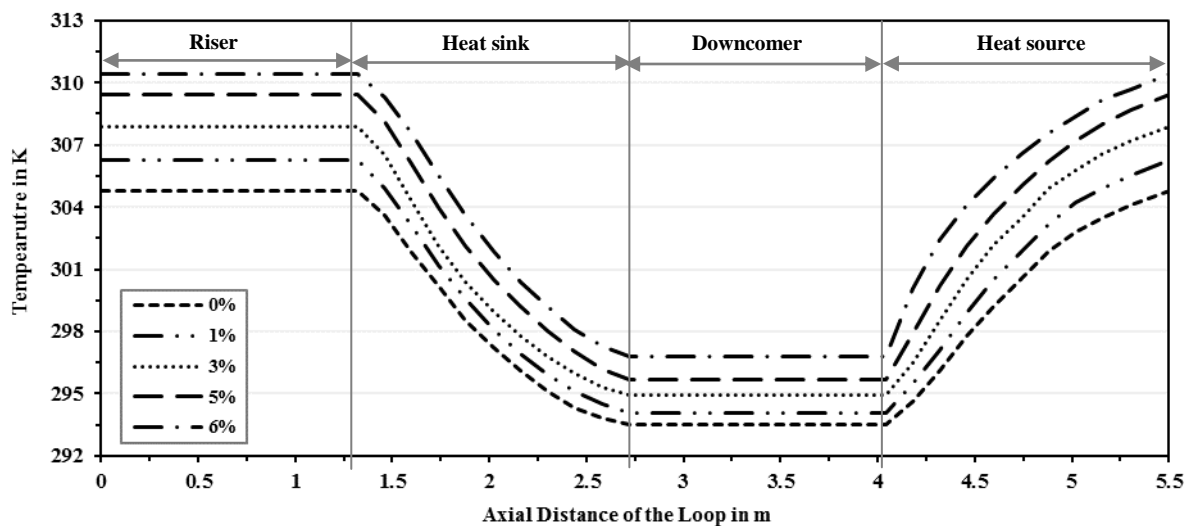


**Figure 7. Temperature profiles along the loop length**

### 5.3 Velocity contours for water and $Al_2O_3$ /water nanofluid at 600W of heat input and 3% concentration

Figs. 6(i) and 6(ii) show the contours of velocity for water and  $Al_2O_3$ /water nanofluid at the center of heat source, riser, heat sink, and down comer respectively. It is clear from the figs. 6(i) and 6(ii), that the velocity at bottom side is more at heat source and the trend is reversed at heat sink due

to buoyancy effect. Relatively more uniform velocity can be observed in case of  $\text{Al}_2\text{O}_3/\text{water}$  nanofluid when compared with water.

#### 5.4 Temperature profiles of the loop fluid along the loop length

Temperature profiles of the water and  $\text{Al}_2\text{O}_3/\text{water}$  nanofluid at different particle volume concentrations for entire loop length at 600W of heat input are shown in fig. 7. Since the riser and downcomer are considered as adiabatic, there is no temperature variation observed in both water and nanofluid. As the heat source is subjected to uniform heat flux, gradual rise in temperature of the loop fluid can be noticed and the trend is reversed for the heat sink.

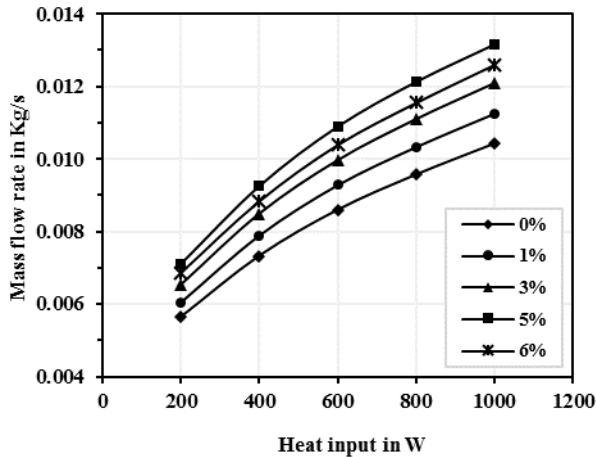


**Figure 8. Variation in steady state mass flow rates with heat input**

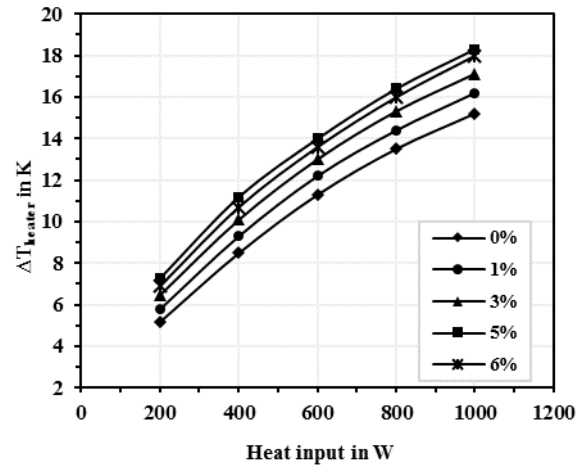


**Figure 9. Variation of temperature gradients across the heat source with heat input**

#### 5.5 Steady state flow rate

The mass flow rate of loop fluid in NCL under steady state condition is obtained at various heat inputs and different particle volume concentrations. It is well known that mass flow rate of the loop fluid increases with increasing heat input at heat source. Fig. 8, explicit the variation of mass of flow rate of water and  $\text{Al}_2\text{O}_3/\text{water}$  nanofluid with heat input. By increasing the heat input to the source, the higher density gradient is developed between the source and sink which causes for enhanced mass flow rate. It is noticed from fig. 8, the mass flow rate of  $\text{Al}_2\text{O}_3/\text{water}$  nanofluid is more than the water with the refined thermo-physical properties. It is observed from the fig. 8, the mass flow rate of loop fluid is enhanced from 7.10% to 26.11% by varying the particle concentration from 1% to 5% when compared with water. But further increasing the particle concentration to 6%, the mass flow rate is decreased by 4.11% as compared with 5% concentration.

The mass flow rate of loop fluid in the NCL is solely influenced by the buoyancy effect. This buoyancy effect can be enhanced either by decreasing the viscous resistive forces or by improving the buoyancy driving forces. The thermo-physical properties of the fluid are influences the viscous forces. Particularly for nanofluid the viscosity has more emphasis on this resistive forces. As the viscosity of nanofluid is a function of the particle volume concentration, its effect cannot be neglected. Therefore, another alternative way to improve the buoyancy driving forces is either by increasing the temperature or by regulating the thermo-physical properties of the fluid. As the particle concentration increases, effective density of the nanofluid is enhanced and specific heat ( $C_p$ ) is reduced. By suspending the nanoparticles in the base fluid, the net specific heat of the nanofluid is reduced [16] as well as thermal expansion



coefficient ( $\beta$ ) of the nanofluid is increased [17] and hence the temperature of loop fluid increases for the same heat input. In the simulation, the specific heat of  $\text{Al}_2\text{O}_3/\text{water}$  nanofluid is estimated using the eq. (10) and the result reveals that, specific heat of the nanofluid is reduced by 3.09%, 8.73% and 14.56% at 1%, 3% and 5% particle volume concentrations respectively when compared with water. This decrease in specific heat gives larger temperature rise in the fluid at the same heat input. The temperature rise gives large change in density gradient between the heat source and heat sink which causes for the increase in mass flow rate. Addition to this, thermal expansion coefficient of the nanofluid is also important parameter for mass flow rate enhancement. Thermal expansion coefficient is more for nanofluid when compared with water. As increasing the particle concentration thermal expansion coefficient is also increases. This may provide a physical reason for the increase of mass flow rate with the addition of nanoparticles up to 5% concentration in water. As the particle concentration increases from 5% to 6%, the percentage increment in viscosity gradients is more than the percentage decrement in the specific heat and therefore, the viscous forces dominates the buoyancy forces. This may be the reason for decrement in the mass flow rate by the addition of nanoparticles beyond 5% particle concentration in water. Therefore, for this NCL model, the particle concentration of 5% is considered as an optimum value.

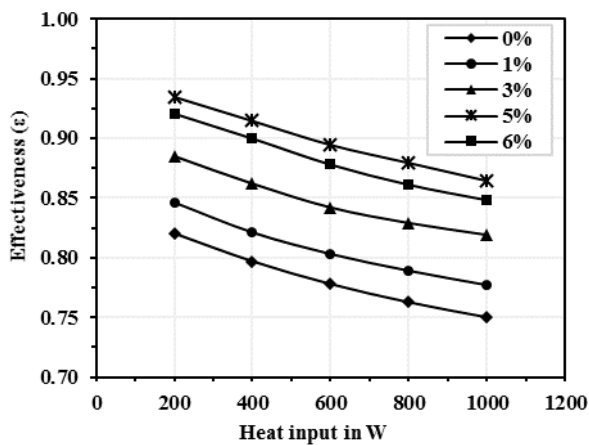


**Figure 10. Variation of effectiveness of the NCL with heat input**

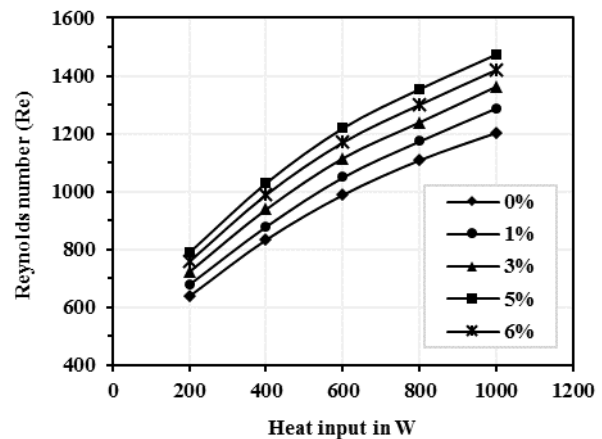


**Figure 11. Variation of Reynolds number with NCL with heat input**

### 5.6 Temperature gradient across the heat source

Fig. 9 shows the variation of temperature gradient across the heat source at different heat inputs and particle concentrations. It is noticed from the fig. 9, the temperature gradient of the loop fluid follows the increasing trend with heat input, whereas this temperature gradient increases with increase of particle concentration up to 5%. But, further increase in particle concentration upto 6%, this temperature gradient is decreased due to decrement in mass flow rate. Fig. 9 clearly shows that, the temperature gradient of the loop fluid across the heat source with nanofluid is higher than water.

### 5.7 Effectiveness of the NCL

Taylor et al. [18] have mentioned that, one can get the clarity on the heat transfer enhancement by non-dimensionalizing the results. Therefore, by defining a non-dimensional parameter called effectiveness ( $\epsilon$ ), the performance of water and nanofluid based NCLs are successfully compared.

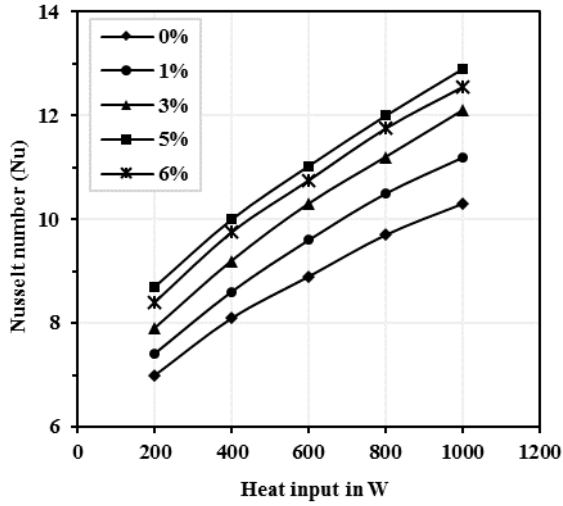


**Figure 12. Variation of Nusselt number with heat input to the source**

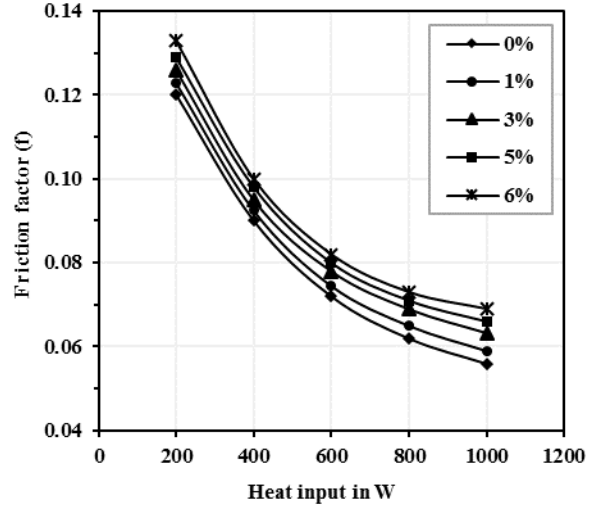


**Figure 13. Variation of friction factor with heat input**

$$\varepsilon = \frac{\dot{m} C_{p1} (T_b - T_a)}{\dot{m} C_{p2} (T_b - T_w)} \quad (23)$$

In the eq. (23),  $T_a$  and  $T_b$  are the temperatures of the loop fluid at the entrance and exit of the heat source and  $T_w$  is the constant wall temperature of the heat sink. Since the fluid flows in a closed loop, the constant mass flow rate is achieved in NCL under steady state condition. Therefore, the mass flow rate terms are removed from eq. (23). In simulations, the specific heats of the loop fluid at source ( $C_{p1}$ ) and sink ( $C_{p2}$ ) are estimated by using eq. (10) and the difference between  $C_{p1}$  and  $C_{p2}$  is obtained less than 0.2%. Hence,  $C_{p1}$  and  $C_{p2}$  terms are neglected in eq. (23). Fig. 10 shows the effect of particle volume concentration and heat input on the effectiveness of NCL. Fig. 10 summarizes that, the effectiveness of the NCL proportionally increases with particle volume concentration. This is also confirmed from the experiments of Doganay et al. [10]. At the higher particle concentrations, specific heat of the nanofluid is reduced and thermal expansion coefficient is increased, consequently the temperature rises in nanofluid increases. Therefore, the higher temperature gradients are created at the heat source. The increment of temperature gradient of the loop fluid across the heat source rises at a higher rate than the temperature difference between loop fluid temperature at source exit and sink wall temperature, hence effectiveness is increased with the particle concentration.

### 5.8 Non-dimensional analysis

Reynolds number can be estimated by eq. (17). Fig. 11 shows the variation of the Reynolds number with heat input and particle volume concentration. Fig. 11 illustrates that, Reynolds number of the nanofluid at any concentration is more than water. By increasing the heat input, the mass flow rate and the subsequent velocities are increased. This increment in fluid velocity causes to increase the Reynolds number.

Nusselt number at the source is calculated based on the area weighted average wall function heat transfer coefficient. The wall function heat transfer coefficient at source is obtained from the simulation results. At the source, a variation of the Nusselt number with heat input and particle volume concentration is shown in fig. 12. The addition of high thermal conductive nanoparticles in the inherently poor conductive water, the effective thermal conductivity of the nanofluid enhances.

Therefore, for a given heat input temperature difference between wall and bulk fluid is less for the nanofluid, which results to increase its heat transfer coefficient. This increment in heat transfer coefficient causes for the enhancement of Nusselt number.

Fig. 13 demonstrates that, friction factor is declines with increase in the heat input because of the temperature gradients dominate the viscous gradients. On the other hand, the friction factor of loop fluid increases with an increase in the particle concentration due to increment in viscosity of the loop fluid.

## 6. Conclusions

In the present study, the steady state analysis has been carried out on the NCL with water and  $\text{Al}_2\text{O}_3$ /water nanofluid at different particle volume concentrations of 1%, 3%, 5% and 6%. A 3-D geometry of the rectangular NCL model is developed and simulated using ANSYS (FLUENT) 14.5. To simulate nanofluid in the NCL, mixture model is adopted because it is computationally less expensive. For the simulations, the imposed thermal boundary conditions are: constant heat input over the range of 200-1000W with step size of 200W at the heat source and isothermal wall temperature of 293K at the heat sink. The adiabatic boundary condition is imposed on both the riser and downcomer. Based on the simulation results, the following conclusions are drawn:

- The steady state mass flow rate of the NCL increases with the heat input.
- As the particle volume concentration increase from 0% to 5%, the mass flow rate in the NCL increases, but further increment in particle concentration reduces the mass flow rate because of viscous forces dominate the buoyancy forces. Therefore, for this kind of NCL model, the particle concentration of 5% is considered as an optimum value.
- Increasing the particle volume concentration from 5% to 6%, the Reynolds number and Nusselt number follow the reverse trend.
- The friction factor of loop fluid in NCL declines with heat input for water and  $\text{Al}_2\text{O}_3$ /water nanofluid and it increases with particle volume concentration.
- Effectiveness of the  $\text{Al}_2\text{O}_3$ /water nanofluid based NCL is more than the water based NCL.

## Acknowledgment

The present work is carried out under a project sponsored by Department of Science and Technology (DST), Ministry of Human Resource and Development (MHRD), Government of India. The financial support offered by MHRD is gratefully acknowledged.

## Nomenclature

A	area ( $\text{m}^2$ )	<i>Greek symbols</i>
d	diameter (m)	$\mu$ dynamic viscosity ( $\text{Ns/m}^2$ )
F	body force (N)	$\phi$ particle volume fraction
g	acceleration due to gravity ( $\text{m/s}^2$ )	
$G_b$	turbulence kinetic energy due to mean buoyancy	<i>subscripts</i>
$G_k$	turbulence kinetic energy due to mean velocity gradient	cs cross section
h	specific enthalpy (J/kg)	eff effective
$L_s$	characteristic length (m)	m mixture
$N_G$	dimensionless parameter ( $= L_t/d$ )	p particle
$\bar{S}$	strain tensor	ss steady state
$\bar{V}_{dr}$	drift velocity (m/s)	t turbulent
$V_s$	characteristic velocity (m/s)	w water

## References

- [1] Y Zvirin, A review of natural circulation loops in pressurized water reactors and other systems, *Nuclear Engineering and Design*, 67 (1981), pp. 203–225
- [2] P K Vijayan, M Sharma, D Saha, Steady state and stability characteristics of single phase natural circulation in a rectangular loop with different heater and cooler orientations, *Experimental Thermal and Fluid Science*, 31 (2007), pp. 925-945
- [3] P K Vijayan, A K Nayak, D S Pilkhwal, D Saha, V Venkat Raj, Effect of loop diameter on the stability of single phase natural circulation in rectangular loops, *Proceedings of the 5th International Topical Meeting on Reactor Thermal Hydraulics (NURETH-5)*, Salt Lake City, USA, (1992), pp. 261-267
- [4] Dipankar N Basu, Souvik Bhattacharyya, P K Das, Development of a unified model for the steady state operation of single phase natural circulation loop, *International Journal of Heat and Mass Transfer*, 62 (2013), pp. 452-462
- [5] Dipankar N Basu, Souvik Bhattacharyya, P K Das. Influence of geometry and operating parameters on the stability response of single phase natural circulation loop, *International Journal of Heat and Mass Transfer*, 58 (2013), pp. 322-334.
- [6] K Kiran Kumar, M Ram Gopal, Steady state analysis of CO<sub>2</sub> based natural circulation loops with end heat exchangers, *Applied Thermal Engineering*, 29 (2009), pp. 1893–1903
- [7] Ajay Kumar Yadav, M Ram Gopal, Souvik Bhattacharyya, CO<sub>2</sub> based natural circulation loops: new correlations for friction and heat transfer, *Int. J. of Heat Mass Tran.*, 55 (2012), pp. 4621-4630
- [8] Jayaraj Tallappa Kudariyawar, Abhijeet Mohan Vaidya, Naresh kumar maheswari, Polepalle Satyamurthy, Computational study of instabilities in a rectangular natural circulation loop using 3D CFD simulation, *International Journal of Thermal Sciences*, 101 (2016), pp. 193-206
- [9] Navak A K, M R Gartia, P K Vijayan, Thermal–hydraulic characteristics of a single phase NCL with water and Al<sub>2</sub>O<sub>3</sub> nanofluids, *Nuclear Engineering and Design*, 239 (2009), pp. 526-540
- [10] Serkan Doganay, Alpaslan Turgut, Enhanced effectiveness of nanofluid based natural circulation mini loop, *Applied Thermal Engineering*, 75 (2015), pp. 669-676
- [11] ANSYS Fluent 15.0 theory guide (2013), 17.2.2.1.2. Significance of the Stokes Number, pp. 471
- [12] M M Rashidi, et al., Comparative numerical study of single and two-phase models of nanofluids heat transfer in wavy channel, *Applied Mathematics and Mechanics*, (2014).
- [13] B E Launder, D B Spalding. The numerical computation of turbulent flow, *Computational Methods in Applied Mechanical Engineering*, 3 (1974), pp. 269–289
- [14] Stern F, Wilson R V, Coleman H W, Paterson E G, Comprehensive approach to verification and validation of CFD simulations-part 1, *Journal of Fluids Engineering*, 123 (2001), pp. 793-802
- [15] P K Vijayan, Experimental observations on the general trends of the steady state and stability behaviour of single-phase natural circulation loops, *Nuclear Engg. Design*, 215 (2002) pp. 139-152
- [16] I C Bang, S H Chang, Boiling heat transfer performance and phenomena of Al<sub>2</sub>O<sub>3</sub>/water nanofluids from a plain surface in a pool, *Int. Jour. of Heat and Mass Transfer*, 48, 12, (2005), pp. 2407-2419
- [17] A K Nayak, R K Singh, P P Kulkarni, Thermal expansion characteristics of Al<sub>2</sub>O<sub>3</sub> nanofluids: more to understand than understood. *Applied Physics Letters*, 94 (2009), pp. 094102:1-3
- [18] Taylor R, et al., Small particles big impacts: a review of the diverse applications of nanofluids, *Journal of Applied Physics*, 113 (2013), pp. 11301-11320